Available online at www.sciencedirect.com
SCIENCE DIRECT
International Journal of Machine Tools & Manufacture 45 (2005) 481–495
INTERNATIONAL JOURNAL OF MACHINE TOOLS & MANUFACTURE DESIGN, RESEARCH AND APPLICATION
www.elsevier.com/locate/ijmactool

Thermal modeling for white layer predictions in finish hard turning

Y. Kevin Chou*, Hui Song

Mechanical Engineering Department, The University of Alabama, Tuscaloosa, AL 35487, USA

Received 7 October 2003; accepted 1 September 2004
Available online 2 November 2004

Abstract

Part thermal damage is a process limitation in finish hard turning and understanding process parameter effects, especially, tool wear, on cutting temperatures is fundamental for process modeling and optimization. This study develops an analytical model for cutting temperature predictions, in particular, at the machined-surfaces, in finish hard turning by either a new or worn tool.

A mechanistic model is employed to estimate the chip formation forces. Wear-land forces are modeled using an approach that assumes linear growth of plastic zone on the wear-land and quadratic decay of stresses in elastic contact. Machining forces and geometric characteristics, i.e. shear plane, chip–tool contact, and flank wear-land, approximate the heat intensity and dimensions of the shear plane, rake face, as well as wear-land heat sources. The three heat sources are further discretized into small segments, each treated as an individual rectangular heat source and subsequently used to calculate temperatures using modified moving or stationary heat-source approaches. Temperature rises due to all heat-source segments are superimposed, with proper coordinate transformation, to obtain the final temperature distributions due to the overall heat sources. All heat sources are simultaneously considered to determine heat partition coefficients, both at the rake face and wear-land, and evaluate the final temperature rises due to the combined heat-source effects.

Simulation results show that, in new tool cutting, maximum machined-surface temperatures are adversely affected by increasing feed rate and cutting speed, but favorably by increasing depth of cut. In worn tool cutting, flank wear has decisive effects on machined-surface temperatures; the maximum temperature increases 2–3 times from 0 to 0.2 mm wear-land width. White layers (phase-transformed structures) formed at the machined-surfaces have been used to experimentally validate the analytical model by investigating tool nose radius effects on the white layer depth. The experimental results show good agreement with the model predictions.

The established model forms a framework for analytical predictions of machined-surface temperatures in finish hard turning that are critical to part surface integrity and can be used to specify a tool life criterion.

Keywords: Hard turning; machined-surface temperature; phase transformation temperature; thermal modeling; tool flank-wear; white layer

1. Introduction

Tool life in finish hard turning is limited by part surface characteristics, e.g. microstructural alterations and surface finish, indirectly correlated to tool wear. Thermal damage due to temperature rises at the machined-surface is the primary source of surface degradation, e.g. side flow [1,2] or white layer [3]. Understanding the complex thermal phenomenon is fundamentally important to deploy efficient thermal management strategies for part damage minimization. In hard turning, due to high specific cutting energy, tool wear growth is rather fast, and, thus, wear-land effects are desirably concerned for process analysis. The presence of flank wear-land accompanies additional cutting forces as well as heat generation to the thermo-mechanical process. Tool wear is detrimental to part quality, in particular, to part surface integrity because of temperature rises at the machined-surface. It has been reported that tool wear is a primary factor to white layer formation, an undesirable by-product, in hard turning [3–5].

Cutting forces due to flank wear-land have been studied by several researchers. There seems to be two schools of thought. One reported chip formation to be independent on wear-land traction, which solely depends on wear-land geometry and cutting conditions [6–9]. One the other hand, Wang and Liu suggested that chip formation forces are affected by wear-land interactions [10,11]. According to Waldorf et al. [6], flank wear-land contact consists of both plastic flow region and elastic contact if the width of wear-

* Corresponding author.
E-mail address: kchou@coe.eng.ua.edu (Y.K. Chou).

0890-6955/$ - see front matter © 2004 Elsevier Ltd. All rights reserved.
doi:10.1016/j.ijmachtools.2004.09.006

Nomenclature

a	angle at lead cutting edge in wear-land geometry model (degree), Fig. 1(b)
A_c	uncut chip area (mm^2)
A_r	area of rake face heat source (mm^2)
A_s	area of shear plane heat source (mm^2)
A_w	area of wear-land heat source (mm^2)
b	angle at tail cutting edge in wear-land geometry model (degree), Fig. 1(b)
CL	contact length between cutting tool and workpiece along the cutting edge
d	depth of cut (mm)
f	feed rate (mm/rev)
F_a	axial cutting force in turning (N)
$F_{a,w}$	axial force component due to wear-land in worn tool cutting (N)
F_f	frictional cutting force at rake face (N)
F_n	normal cutting force at rake face (N)
F_{PW}	cutting force due to wear-land (N)
F_{QW}	thrust force due to wear-land (N)
F_r	radial cutting force in turning (N)
$F_{r,w}$	radial force component due to wear-land in worn tool cutting (N)
F_s	shear force on shear plane (N)
F_t	tangential cutting force in turning (N)
$F_{t,w}$	tangential force component due to wear-land in worn tool cutting (N)
h_θ	uncut chip thickness as a function of location across the cutting edge (mm)
k	thermal conductivity of workpiece (W/m K)
k_t	thermal conductivity of cutting tool (W/m K)
K_f	specific frictional pressure (N/mm^2)
K_n	specific normal pressure (N/mm^2)
l_r	tool chip contact length as a function of location across the cutting edge (mm)
l_s	shear plane length as a function of location across the cutting edge (mm)
q_r	heat flux of rake face heat source (W/m^2)
q_s	heat flux of shear plane heat source (W/m^2)
q_w	heat flux of wear-land heat source (W/m^2)
r	tool nose radius (mm)
ΔS_θ	discretized shear plane heat source
$\Delta S'_\theta$	image heat source of discretized shear plane heat source
t_θ	chip thickness as a function of location across the cutting edge (m)
T_0	initial tool and workpiece temperature (20 °C)
T_c	temperature in a chip (°C)
$T_{c,r}$	temperature rise in chip due to rake face heat source (°C)
$T_{c,s}$	temperature rise in chip due to shear plane heat source (°C)
T_t	temperature in a tool (°C)
$T_{t,r}$	temperature rise in tool due to rake face heat source (°C)
$T_{t,w}$	temperature rise in tool due to wear-land heat source (°C)
T_w	temperature in a workpiece (°C)
$T_{w,s}$	temperature rise in workpiece due to shear plane heat source (°C)
$T_{w,w}$	temperature rise in workpiece due to wear-land heat source (°C)
$\Delta T_{c,r}$	temperature rise in chip due to rake face heat source (°C)
$\Delta T_{c,s}$	temperature rise in chip due to shear plane heat source (°C)
$\Delta T_{t,r}$	temperature rise in cutting tool due to rake face heat source (°C)
$\Delta T_{w,s}$	temperature rise in workpiece due to shear plane heat source (°C)
V	cutting speed (m/s)
V_c	cutting chip speed (m/s)
V_s	shear plane speed (m/s)
VB	width of flank wear (mm)
VB_P	width of plastic flow region on flank wear (mm)
α	rake angle (rad)
α_0	nominal rake angle (rad)
β_r	heat partition coefficient of rake face heat source
β_w	heat partition of for wear-land heat source
χ	thermal diffusivity (m^2/s)
ϕ	shear angle (rad)
σ_0	normal stress at plastic flow region of flank wear-land (N/m^2)
σ_w	normal stress at elastic region of flank wear-land (N/m^2)
τ_0	shear stress at plastic flow region of flank wear-land (N/m^2)
τ_s	shear flow stress on shear plane (N/m^2)
τ_w	shear stress at elastic region of flank wear-land (N/m^2)
θ	a variable (angle) to define location across the cutting edge
θ_1	θ associated with tail cutting edge (rad)
θ_2	θ associated with lead cutting edge (rad)

land, VB, is greater than a certain level VB_{cr}. Smithey et al. [7,8] further proposed that the width of plastic flow region (VB_P) linearly increases with VB and the proportionality is independent of cutting conditions, but solely a function of the workpiece and cutting tool materials. Following the assumption of the linear growth of plastic zone, stresses are modeled to be constant in plastic flow region and quadratic distribution in elastic contact. Once normal and

shear stresses are determined, cutting forces due to tool wear can be obtained by integrating stresses over the flank wear-land area. Elanayar and Shin also studied cutting forces due to wear-land using an indentation force model [9]. The authors also reported that wear-land effects on chip formation forces are insignificant. Huang and Liang have applied the worn tool model from [6–8], expanding to three-dimensional cutting, to model wear-land forces in hard turning [12] and reported that model predictions agree with experimental results in a wide range of cutting conditions.

Wang and Liu [10] developed a method to decouple wear-land forces and chip formation forces. A thermal model based on Green's function was developed and, by using white layer thickness in the chip (free surface side) as the thermal boundary condition of the machined-surface (in orthogonal cutting), average stresses attributed to wear-land traction can be determined. The results indicate influence of wear-land to chip formation forces. The authors further characterized wear-land effects on heat transfer of chip formation and part surface microstructural alterations in orthogonal cutting [11]. Cutting chip and workpiece temperature rises due to shear plane heating, however, were neglected in the analysis.

Cutting temperature has been frequently studied in machining theory and practices including analytical approaches, finite element/difference methods, and experimental temperature measurements, etc. Recent advances of analytical modeling for cutting temperatures were due to Komanduri and Hou [13–15]. The authors proposed to use modified Hahn's moving oblique band heat source solution [16] with appropriate image heat source for the shear plane heat source effects on workpiece temperature rise. Moreover, modified Jaeger's moving band and stationary rectangular heat source solutions [17] were used for the chip and tool, respectively, again with appropriate image heat sources.

Conventional thermal models usually target the cutting tool temperatures and are mostly two-dimensional without tool nose radius concerned, suitable for roughing applications. Furthermore, the workpiece considered in the conventional models is indeed transient materials to be removed in subsequent revolutions during machining, not significantly related to the final machined-surface. In finish hard turning, the cutting is mainly engaged in the tool nose radius area that results in three dimensional cutting configurations, i.e. variable uncut chip geometry, and variable distance from the cutting edge to the machined-surface too, across the cutting edge.

The overall goal of this study is to develop a thermal model for temperature predictions in finish hard turning, in particular, the machined-surface temperature that can be used for part thermal damage evaluation. The mechanistic approach is used to model chip formation forces and linear growth of plastic zone is adopted to model wear-land forces. Cutting mechanics is used to obtain the heat sources information. Discretization of the heat sources is applied and each small heat source segment is then individually used to study the temperature rise during machining, using modified moving and stationary heat-source approaches developed by Komanduri and Hou [13,14]. Superposition of temperature rise due to all small heat-source segments yields the final temperature distributions due to overall heat sources. Parametric study is conducted with emphasis on the machined-surface temperatures as practical guidelines for tool life determination.

2. Machining force model

2.1. Chip formation forces

Fig. 1 shows a sketch of an uncut chip in finish hard turning. Uncut chip area, A_c, and cutting edge contact length, CL (arc AB), are functions of cutting parameters and the tool nose radius, so is the uncut chip thickness (h_θ) across the cutting edge [18]. The uncut chip area is composed of numerous thin slices (Fig. 1), each with dimensions of uncut chip thickness (h_θ, a variable) and infinitesimally small width ($\delta w = r\delta\theta$). The mechanistic approach is then applied to relate normal and friction forces (δF_n and δF_f) at the rake with uncut chip area (δA_c) and two specific cutting pressure constants, K_n and K_f. The selected predictors for K_n and K_f models, suggested from the regression results, are as follows

$$\ln(K_n) = a_0 - a_1 \ln(\bar{h}_\theta) - a_2 \ln(V) - a_3 \ln(\gamma_e) - a_4 \ln(\mathrm{CL}),$$
$$\ln(K_f) = b_0 - b_1 \ln(\bar{h}_\theta) + b_2 \ln(V) - b_3 \ln(\gamma_e) - b_4 \ln(CL). \quad (1)$$

By proper coordinate transformation, cutting forces due to an individual uncut chip slice at θ can be projected to the global cutting coordinated system, i.e. tangential, radial, and axial components. Further integrating forces from the lead to tail cutting edges results in overall three components of cutting forces, measurable by a force sensor.

A set of machining experiments with cutting force measurements is needed to determine constants in specific pressure terms using regression means and then used for chip-formation force predictions [19].

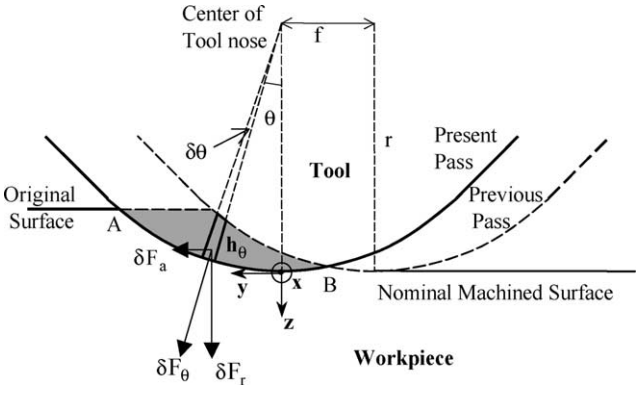

Fig. 1. Sketch showing uncut chip geometry in finish hard turning.

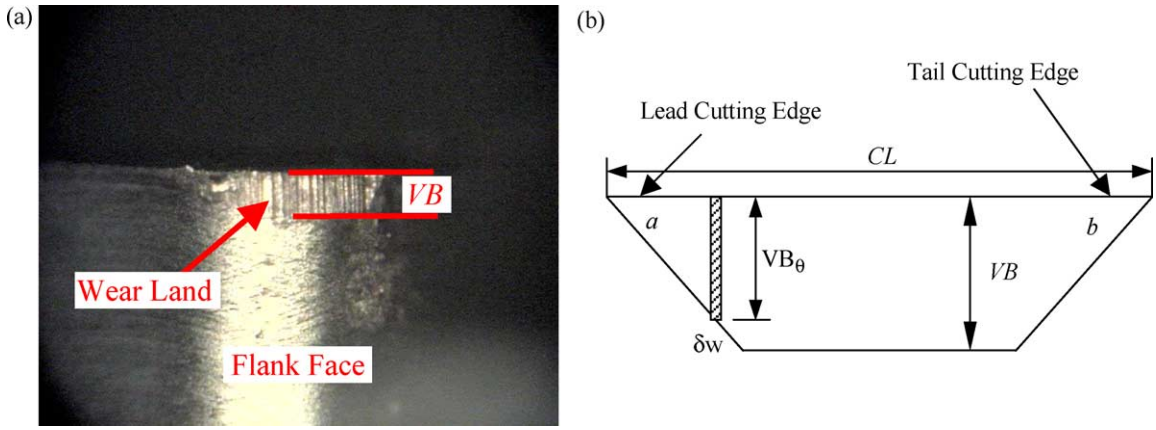

Fig. 2. (a) Optical micrograph of flank wear-land of a worn tool and (b) flat depiction of flank wear-land.

2.2. Wear-land forces

A typical flank wear-land of a worn cutting tool in finish hard turning is shown in Fig. 2(a). Fig. 2(b) shows flank wear-land spread out as a flat section. The angles a and b range from 55 to 70° and 45 to 65°, respectively, based on experimental observations. The wear-land contact is composed of a number of small slices as shown in Fig. 2(b). Differential cutting forces, δF_{PW} and δF_{QW}, due to a small wear-land slice can be calculated by integrating normal and shear stresses over the area of thecorresponding slice

$$\begin{aligned}\delta F_{PW} &= \mathrm{VB_P}\delta w\tau_0 + \int_{\mathrm{VB_P}}^{\mathrm{VB}_\theta}\delta w\tau_w(x)\mathrm{d}x,\\ \delta F_{QW} &= \mathrm{VB_P}\delta w\sigma_0 + \int_{\mathrm{VB_P}}^{\mathrm{VB}_\theta}\delta w\sigma_w(x)\mathrm{d}x.\end{aligned} \tag{2}$$

In elastic contact, the stresses decrease as a parabolic fashion toward the end of contact ($x=\mathrm{VB}$), [7]

$$\begin{aligned}\sigma_w(x) &= \sigma_0\left(\frac{\mathrm{VB}-x}{\mathrm{VB}-\mathrm{VB_p}}\right)^2,\\ \tau_w(x) &= \tau_0\left(\frac{\mathrm{VB}-x}{\mathrm{VB}-\mathrm{VB_p}}\right)^2.\end{aligned} \tag{3}$$

σ_0 and τ_0 are related to the flow stress on the shear plane and determined from the slip-line field theory [7,20].

Differential forces due to stresses over the wear-land slice can then be transformed to the global coordinate system (workpiece) and integrated to obtain three components of wear-land forces, i.e. radial ($F_{r,w}$), tangential ($F_{t,w}$), and axial ($F_{a,w}$) components.

Equations above evaluate the wear-land forces at different machining conditions and, together with the new tool chip-formation forces that are assumed independent on the wear-land, establish the overall machining force model in finish hard turning using a worn tool.

3. Temperature modeling

Modeled machining forces and cutting geometry information, i.e. shear angle, chip–tool contact, and wear-land shape, empirically obtained, are used to estimate the heat intensity of the three heat sources. The cutting geometry, i.e. the shear plane and chip–tool contact, is further assumed not affected by flank wear-land, and, thus, the shear plane and rake face heat sources can be defined based on the new tool machining conditions. As the heat sources are three dimensional, they are further discretized into small segments. Each heat-source segment will then be considered as an individual rectangular heat source for temperature rise calculations in the workpiece, chip, and tool, using modified heat source approaches developed by Komanduri and Hou [13,14]. Superposition is then applied to estimate the overall temperature rises due to the entire heat sources.

3.1. Shear plane heat source

The heat intensity of shear plane heat source is $q_s = F_s V_s/A_s$; F_s and V_s are shear force and shear plane speed from classical cutting mechanics analysis, and $A_s = \int_{\theta_1}^{\theta_2} r l_s(\theta)\mathrm{d}\theta$ is the area of shear plane, and l_s, varying across the cutting edge (Fig. 3), is estimated as $l_s(\theta) = h_\theta/\sin\phi$. Constant shear angle is assumed across the chip width and shear plane length continuously varies across the cutting edge. The shear angle required for shear force and shear plane length and speed calculations is approximated from a mechanistic model as an implicit form [19,21].

For shear plane heating, the thermal phenomenon is equivalent to material flowing through a heating zone and can be analyzed by material flow and heat transport [13]. For the workpiece temperature rise due to shear plane heat source, according to Komanduri and Hou [13], chip and cutting tool existence is negligible by virtually filling the workpiece in the cut area behind the shear plane to render a straight boundary of a semi-infinite medium. Assuming an adiabatic surface, the problem is mathematically equivalent to adding an imaginary oblique plane heat source in an imaginary infinite half-space. Hence, the problem turns into two oblique heat sources moving in an infinite body, analytically solvable from heat conduction theory.

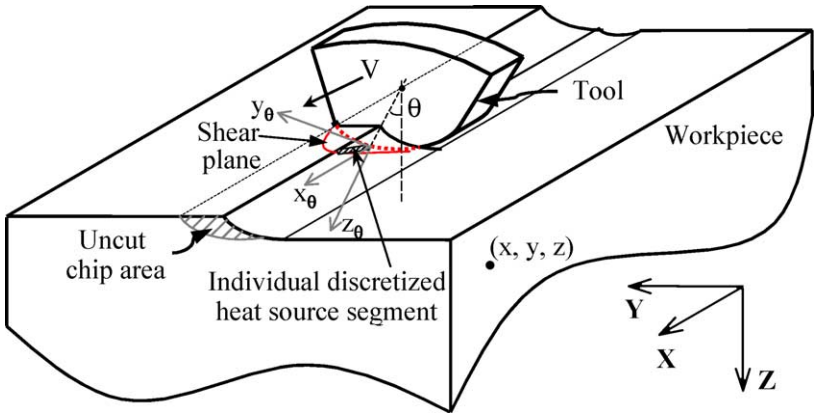

Fig. 3. Discretization of the shear plane heat source.

The shear plane heat source is discretized into a number of small two-dimensional rectangular heat source segments, each with a length of $l_s(\theta)$ and width δw. Each individual small heat source is then modeled as an oblique rectangular heat source ΔS_θ moving at the cutting speed on the workpiece with the shear angle as the oblique angle [13]. In modeling individual heat-source segments, because the width of segments is far smaller compared to the arc of the transient machined-surface (due to tool nose radius), which is part of the surface boundary of the semi-infinite body (workpiece), the surface is further assumed to have zero curvature, Fig. 4. A combination of Polar and Cartesian coordinate systems is introduced to evaluate the distance of points to the heat source segments for the temperature rise calculations.

The temperature rise, of quasi-steady state, in the workpiece due to an oblique rectangular heat sources ΔS_θ as well as the imaginary counterpart is, therefore

$$\Delta T_{w,s}(x_\theta, y_\theta, z_\theta) = \frac{q_s}{4\pi k}\int_{x_\theta}^{x_\theta + l_s\cos\phi} e^{-V\eta/2\chi}\,d\eta \int_{y_\theta-\delta w/2}^{y_\theta+\delta w/2} \frac{\exp\left(-V\sqrt{\left[\eta^2+\zeta^2+\left(z_\theta - h_\theta + \frac{\eta - x_\theta}{l_s\cos\phi}h_\theta\right)^2\right]}/2\chi\right)}{\sqrt{\left[\eta^2+\zeta^2+\left(z_\theta - h_\theta + \frac{\eta - x_\theta}{l_s\cos\phi}h_\theta\right)^2\right]}}\,d\zeta$$
$$+ \frac{q_s}{4\pi k}\int_{x_\theta}^{x_\theta + l_s\cos\phi} e^{-V\eta/2\chi}\,d\eta \int_{y_\theta-\delta w/2}^{y_\theta+\delta w/2} \frac{\exp\left(-V\sqrt{\left[\eta^2+\zeta^2+\left(z_\theta + h_\theta - \frac{\eta - x_\theta}{l_s\cos\phi}h_\theta\right)^2\right]}/2\chi\right)}{\sqrt{\left[\eta^2+\zeta^2+\left(z_\theta + h_\theta - \frac{\eta - x_\theta}{l_s\cos\phi}h_\theta\right)^2\right]}}\,d\zeta. \quad (4)$$

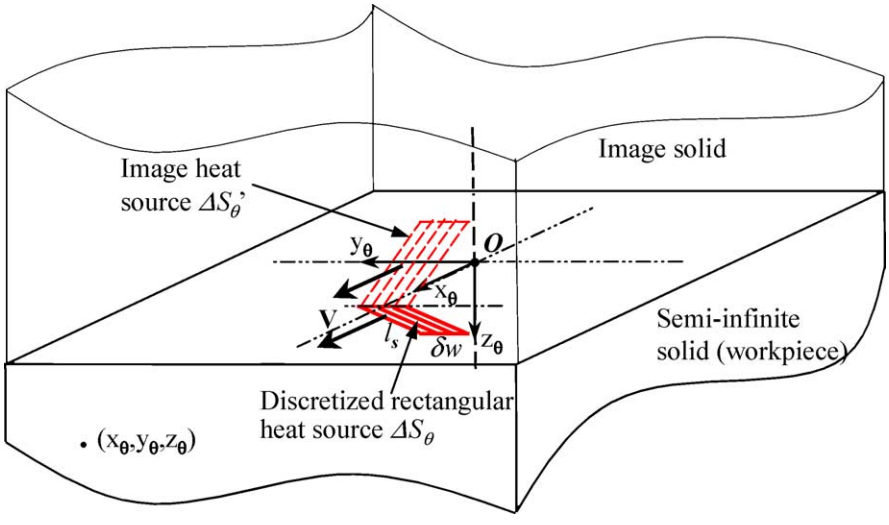

Fig. 4. Moving oblique heat-source model for workpiece temperature rise due to an individual shear plane heat-source segment.

Coordinates with subscript θ indicate the local heat-source segment coordinate system (Fig. 3), x_θ along the cutting direction, y_θ tangential to the cutting edge at location θ, z_θ along the tool nose radial direction at location θ. Such coordinate system changes with θ from the lead to tail cutting edges. Temperature rise at any point (x, y, z) in the workpiece due to the entire shear plane heat source is then the superposition of temperature increases due to all small rectangular heat source segments, i.e.

$$T_{\mathrm{w}}(x,y,z) = \sum_{\theta_1}^{\theta_2} \Delta T_{\mathrm{w,s}}(x,y,z) + T_0 = \sum_{\theta_1}^{\theta_2} \Delta T_{\mathrm{w,s}}(x_\theta, y_\theta, z_\theta) + T_0. \quad (5)$$

For the temperature rise in the chip due to the shear plane heat source, similar approach from Komanduri and Hou [13] is adopted. The chip body is virtually extended from the shear plane into the workpiece, infinite along and opposite to the chip flow direction. The free surface of the chip is considered adiabatic, and, thus, an imaginary heat source and semi-infinite chip body are placed symmetric to the chip free surface. The shear plane heat source, with its imaginary part, is then treated as an oblique heat source moving in an infinite body with the cutting chip speed. Similarly, the shear plane heat source is discretized and used for temperature rise calculation in the chip body, Eq. (6) below

$$\Delta T_{\mathrm{c,s}}(x_\theta,y_\theta,z_\theta) = \frac{q_{\mathrm{s}}}{4\pi k}\int_{x_\theta}^{x_\theta + l_{\mathrm{s}}\sin(\phi-\alpha)} \mathrm{e}^{-V_{\mathrm{c}}\eta/2\chi}\,\mathrm{d}\eta \int_{y_\theta-\delta w/2}^{y_\theta+\delta w/2} \frac{\exp\left(-V_{\mathrm{c}}\sqrt{\left[\eta^2+\zeta^2+\left(z_\theta - t_\theta + \frac{\eta - x_\theta}{l_{\mathrm{s}}\sin(\phi-\alpha)}t_\theta\right)^2\right]}/2\chi\right)}{\sqrt{\left[\eta^2+\zeta^2+\left(z_\theta - t_\theta + \frac{\eta - x_\theta}{l_{\mathrm{s}}\sin(\phi-\alpha)}t_\theta\right)^2\right]}}\mathrm{d}\zeta$$
$$+ \frac{q_{\mathrm{s}}}{4\pi k}\int_{x_\theta}^{x_\theta + l_{\mathrm{s}}\sin(\phi-\alpha)} \mathrm{e}^{-V_{\mathrm{c}}\eta/2\chi}\,\mathrm{d}\eta \int_{y_\theta-\delta w/2}^{y_\theta+\delta w/2} \frac{\exp\left(-V_{c}\sqrt{\left[\eta^2+\zeta^2+\left(z_\theta + t_\theta - \frac{\eta - x_\theta}{l_{\mathrm{s}}\sin(\phi-\alpha)}t_\theta\right)^2\right]}/2\chi\right)}{\sqrt{\left[\eta^2+\zeta^2+\left(z_\theta + t_\theta - \frac{\eta - x_\theta}{l_{\mathrm{s}}\sin(\phi-\alpha)}t_\theta\right)^2\right]}}\mathrm{d}\zeta. \quad (6)$$

Superposition of temperature rise due to all individual heat-source segments further determines the temperature rise in the chip due to the entire shear plane heat source.

3.2. Rake face heat source

For rake face heating, the thermal phenomenon is a typical sliding contact problem. The heat intensity of the rake face heat source is $q_{\mathrm{r}} = F_{\mathrm{f}}V_{\mathrm{c}}/A_{\mathrm{r}}$; F_{f} and V_{c} are the frictional force at the rake face and cutting chip speed, and A_{r} is tool–chip contact area. The tool–chip contact length in finish hard turning also varies across the cutting edge. To formulate tool–chip contact length, l_{r}, a linear relationship is assumed as the tool–chip contact length at any location, θ, proportional to the uncut chip thickness h_θ, i.e. $l_{\mathrm{r}}(\theta) = K_1 h_\theta + K_2$. The constant and proportionality are dependent upon cutting parameters. This approach is further modified based on experimental observations. From machining tests and measurements, a relationship is established as below

$$l_{\mathrm{r}}(\theta) = \left(1.75 - \frac{\ln(V)}{3}\right)h_\theta + 0.015. \quad (7)$$

Thus, the tool–chip contact area, A_{r}, is $A_{\mathrm{r}} = \int_{\theta_1}^{\theta_2} l_{\mathrm{r}}(\theta)\mathrm{d}\theta$.

Frictional heat at the tool rake face results in temperature rise in both the chip and cutting tool. Thus, a heat partition coefficient, β_{r} to the tool, is introduced, and will be later determined by matching the average interface temperature. It is further assumed that the heat intensity is uniformly distributed and heat partition coefficient is constant across the contact. The discretization method will be again applied to create a number of small heat segments. For the temperature rise due to an individual heat-source segment, tool nose curvature is again considered to be zero (flat surface boundary) The heat segment with partial heat flux, $\beta_{\mathrm{r}}q_{\mathrm{r}}$, can then be used as a stationary heat source to evaluate the temperature rise in the tool, assuming the tool being a semi-infinite body. Jaeger's solution for rectangular stationary heat sources [17] can then be applied for the temperature rise at any point $(x_\theta, y_\theta, z_\theta)$ due to an individual heat-source segment with dimensions of $l_{\mathrm{r}}(\theta)$ and $r\delta\theta$, and heat flux $\beta_{\mathrm{r}}q_{\mathrm{r}}$

$$\Delta T_{\mathrm{t,r}}(x_\theta,y_\theta,z_\theta) = \frac{\beta_{\mathrm{r}}q_{\mathrm{r}}}{2\pi k_{\mathrm{t}}}\int_0^{l_{\mathrm{r}}}\mathrm{d}\zeta\int_{-\delta w/2}^{\delta w/2}\left[\sqrt{x_\theta^2+(y_\theta-\eta)^2+(z_\theta-\zeta)^2}\right]^{-1}\mathrm{d}\eta. \quad (8)$$

The temperature rise at any point (x, y, z) in the cutting tool due to the entire rake face heat source can then be approximated as the summation of Eq. (8) over the tool–chip contact area.

For the temperature increase in the chip due to frictional heat at the rake face, the heat source, $(1-\beta_{\mathrm{r}})q_{\mathrm{r}}$ and A_{r}, is considered as a moving source of heat on the tool–chip

contact. To apply the moving heat source approach, the chip body is again modified as in the shear plane heat source model, i.e. extending the chip body over the shear plane and placing an equal heat flux and chip body mirror to the chip free surface (adiabatic boundary) [14]. Following similar approach, the temperature rise in the chip due to an individual rectangular heat source segment, dimensions of $l_r(\theta)$ and δw, and heat flux $(1-\beta_r)q_r$, is

$$\Delta T_{c,r}(x_\theta, y_\theta, z_\theta) = \frac{(1-\beta_r)q_r}{2\pi k}\left[\int_{x_\theta - l_r}^{x_\theta + l_r} e^{-V_c\eta/2\chi}\, d\eta \int_{y_\theta - \delta w/2}^{y_\theta + \delta w/2} \frac{\exp\left(-V_c\sqrt{((\eta - x_\theta)^2 + (\zeta + y_\theta)^2 + z_\theta^2)}/2\chi\right)}{\sqrt{((\eta - x_\theta)^2 + (\zeta - y_\theta)^2 + z_\theta^2)}} d\zeta \right.$$
$$\left. + \int_{x_\theta - l_r}^{x_\theta + l_r} e^{-V_c\eta/2\chi}\, d\eta \int_{y_\theta - \delta w/2}^{y_\theta + \delta w/2} \frac{\exp\left(-V_c\sqrt{((\eta - x_\theta)^2 + (\zeta + y_\theta)^2 + (z_\theta + 2t_\theta)^2)}/2\chi\right)}{\sqrt{((\eta - x_\theta)^2 + (\zeta - y_\theta)^2 + (z_\theta + 2t_\theta)^2)}} d\zeta \right]. \quad (9)$$

Superposition of the results from Eq. (9), at different θ's is to estimate temperature rise at any point (x, y, z) in the chip due to the entire rake face heat source. The overall temperature rise in the chip due to both shear plane and rake face heat sources is the numerical sum of individual effects

$$T_c(x,y,z) = \sum_{\theta_1}^{\theta_2} \Delta T_c(x,y,z) + T_0$$
$$= \sum_{\theta_1}^{\theta_2} \Delta T_{c,s}(x_\theta, y_\theta, z_\theta) + \sum_{\theta_1}^{\theta_2} \Delta T_{c,r}(x_\theta, y_\theta, z_\theta) + T_0. \quad (10)$$

3.3. Wear-land heat source

From wear-land force analysis, heat intensity of wear-land heat source, q_w, can be formulated as:

$$q_w(x) = \tau_0 V \quad \text{in plastic flow region } 0 \le x \le VB_P,$$
$$q_w(x) = \tau_w(x) V \quad \text{in elastic contact } VB_P \le x \le VB. \quad (11)$$

A heat partition coefficient, β_w, is also needed to define the fraction of wear-land heat generation that conducts into the tool. The wear-land heat intensity for workpiece temperature analysis is, therefore $(1-\beta_w)q_w$.

Similar to the shear plane and rake face, wear-land heat source is discretized across the cutting edge, composing small radial segments, each with dimensions of VB_θ and width $r\delta\theta$. Jaeger's moving and stationary heat-source theories are then employed to calculate cutting temperatures due to individual heat-segments. The boundary of the workpiece surface, transient surface portion, is considered to be flat (zero curvature) and infinite, Fig. 5. In addition, the worn tool geometry is assumed as a semi-infinite body with the relief face as the boundary. Coordinate transformation

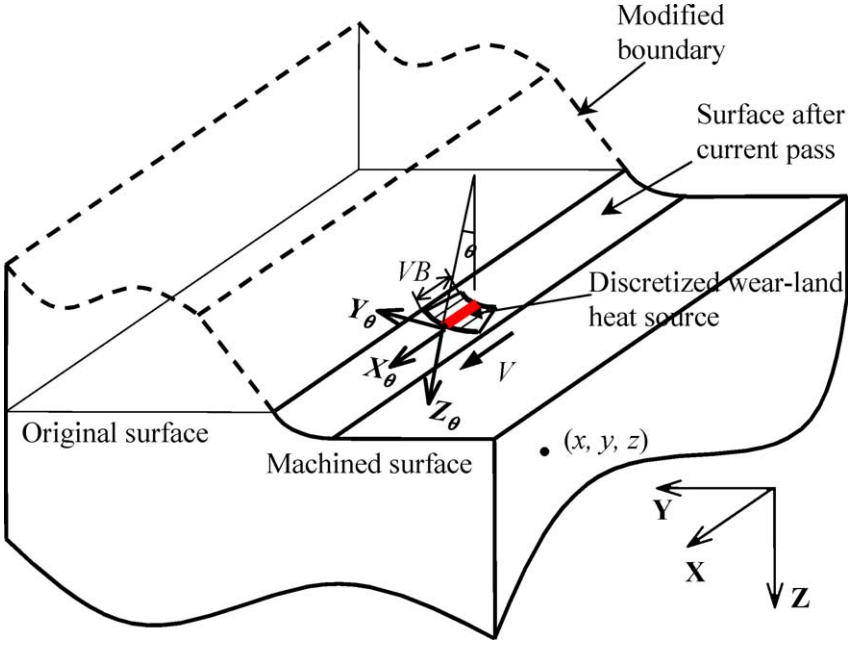

Fig. 5. Descritization of the wear-land heat source and boundary condition modified for workpiece temperature analysis.

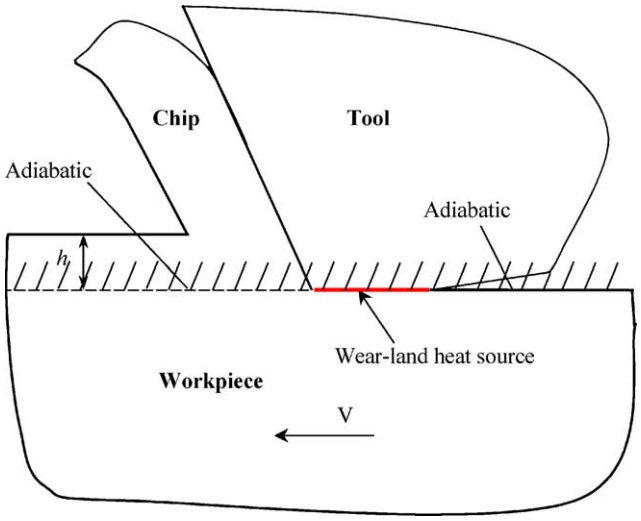

Fig. 6. Modeling of individual wear-land heat source segment for the workpiece temperature analysis.

between local (heat-segment) and global (workpiece) systems, for any heat-source segment at θ, is facilitated for the ease of computation.

For any individual heat-source segment, the wear-land sliding on the workpiece is shown, in two-dimensional view, in Fig. 6. As heat source has very minor effects on materials in front of it, workpiece material that is above the cut surface and in front of shear plane can be neglected, while imposing an adiabatic boundary surface extended from the cut surface and wear-land. The problem is then a heat-source moving (with cutting speed, V) on the workpiece surface, applicable to Jaeger's theory. The workpiece temperature rise at any point (x_θ, y_θ, z_θ) in a semi-infinite solid (workpiece) due to an individual discretized wear-land heat segment at θ is:

$$\Delta T_{w,w}(x_\theta,y_\theta,z_\theta)=\frac{(1-\beta_w)}{2\pi k}\int_{x_\theta}^{x_\theta+VB_\theta} e^{-V\eta/2\chi}q_w(\eta)d\eta \times\int_{y_\theta-\delta w/2}^{y_\theta+\delta w/2}\frac{\exp\left(-V\sqrt{(\eta^2+\zeta^2+z_\theta^2)}/2\chi\right)}{\sqrt{(\eta^2+\zeta^2+z_\theta)}}d\zeta. \quad (12)$$

Superposition of the workpiece temperature increases due to all small segments of shear plane heat source, Eq. (4), and wear-land heat source, Eq. (12), gives the temperature rise in the workpiece in worn tool cutting

$$T_w(x,y,z)=\sum_{\theta_1}^{\theta_2}\Delta T_w(x,y,z)+T_0 =\sum_{\theta_1}^{\theta_2}[\Delta T_{w,s}(x_\theta,y_\theta,z_\theta)+\Delta T_{w,w}(x_\theta,y_\theta,z_\theta)]+T_0. \quad (13)$$

Similarly, portion of wear-land heating can be considered as a stationary heat source on the relief face of the cutting tool, assumed as a semi-infinite body. Thus, the temperature rise in the tool due to a discretized wear-land heat segment can be calculated as:

$$\Delta T_{t,w}(x_\theta,y_\theta,z_\theta)=\frac{\beta_w}{2\pi k_t}\int_{-VB_\theta/2}^{VB_\theta/2}q_w(\zeta)d\zeta \times\int_{-\delta w/2}^{\delta w/2}\left[\sqrt{x_\theta^2+(y_\theta-\eta)^2+(z_\theta-\zeta)^2}\right]^{-1}d\eta. \quad (14)$$

Tool temperature rise in worn tool cutting is, therefore, due to the combined effects of the rake face and wear-land heat sources

$$T_t(x,y,z)=\sum_{\theta_1}^{\theta_2}\Delta T_t(x,y,z)+T_0 =\sum_{\theta_1}^{\theta_2}[\Delta T_{t,r}(x_\theta,y_\theta,z_\theta)+\Delta T_{t,w}(x_\theta,y_\theta,z_\theta)]+T_0. \quad (15)$$

Heat partition coefficients, β_r and β_w, are determined, simultaneously, by matching the average temperatures at tool (rake)–chip interface and tool (flank)–workpiece interface.

Once the heat partition coefficients are determined, temperature rises in the workpiece, cutting tool, and chip can be finally calculated by superposition of temperature increase due to the three heat sources using the determined fractional intensity.

4. Analysis results

4.1. Chip formation forces

A set of hard turning experiments has been performed with cutting force measurements to calibrate K_n and K_f. Ceramic cutting tools, alumina and titanium carbide composite (AlTiC), with 20°×0.1 mm chamfer were used. Cutting geometry was −5° nominal rake angle, 5° relief angle, and 15° both side and end cutting edge angles. Tool nose radius tested included 0.8, 1.6, and 2.4 mm. Workpieces are solid round bars made of through hardened AISI 52100 steel, 60–62 HRc. Outside diameter turning without cutting fluid was performed on a 10 hp precision CNC lathe. Machining parameters ranged from 1 to 4 m/s of cutting speed, 0.025 to 0.6 mm/rev feed rate, and 0.05 to 0.4 mm depth of cut. A triaxial dynamometer with data acquisition was used to record three components of cutting forces.

K_n and K_f of each cutting condition can be derived based on cutting forces data. Using the least square regression method, all the coefficients of K_n and K_f can be determined. As indicated before, other than average uncut chip thickness and cutting speed, cutting edge contact length and effective lead angle also strongly influence

cutting forces. The regression results suggested K_n and K_f to be formulated as

$$\begin{aligned}\ln(K_n) &= 7.54 - 0.329\ln(\bar{h}_\theta) - 0.0222\ln(V) \\ &\quad - 0.229\ln(\gamma_e) - 0.06\ln(\mathrm{CL}), \\ \ln(K_f) &= 5.72 - 0.515\ln(\bar{h}_\theta) + 0.123\ln(V) \\ &\quad - 0.474\ln(\gamma_e) - 0.142\ln(\mathrm{CL}).\end{aligned} \tag{16}$$

The mechanistic model above shows R-squared values of 93.9 and 90.4%, respectively [19].

4.2. Wear-land forces

Wear-land traction forces can be simulated at different machining conditions, also different wear-land geometry due to different tool nose radii. Wear-land dimensions are defined by CL, VB as well as two angles, a and b, at the lead and tail cutting edges, assumed to be 65 and 55° in the current analysis. In addition, tool–workpiece contact length across the cutting edge, CL, is a function of depth of cut and the tool nose radius. Shear flow stress on the shear plane has been established from the mechanistic force model in new tool cutting and is used to estimate normal and shear stresses in the plastic contact area at the wear-land. Based on experimental observations, the entire wear-land is further assumed to be elastic contact, i.e. $\mathrm{VB} < \mathrm{VB}_{cr}$, when VB is less than 0.3 mm. The simulation results show that wear-land forces linearly increase with the width of wear-land, VB, because the force components are proportional to the area of the flank wear-land [20].

4.3. Machined-surface temperatures

The thermal model has been used to study the workpiece, tool, and chip temperatures in finish hard turning of AISI 52100 steel using a worn AlTiC tool. It is known that thermal properties are temperature dependent. However, to apply moving and stationary heat source approach and superposition, the thermal model developed in this study has assumed the problem to be linear. Thus, constant thermal properties at an equivalent temperature are needed for temperature calculations. For workpiece and chip temperature increases due to the shear plane heat source, the equivalent temperature is considered as the average of mean shear plane temperature and initial workpiece temperature [13]. For tool and chip temperature rise due to the rake face heat source, the equivalent temperature used was the initial temperature [14]. For workpiece temperature analysis due to the wear-land heat source, the equivalent temperature is considered as the average of mean wear-land contact temperature (workpiece side) and initial workpiece temperature. For tool temperature rise due to wear-land heat source, the initial tool temperature is used. For AISI 52100 steel, temperature dependent thermal properties below were used [22]

$$\begin{aligned}k(T) &= 45.68 - 0.024T, \\ \chi(T) &= \frac{0.0497}{3T + 2500} - 6.057\times10^{-6}.\end{aligned} \tag{17}$$

Thermal conductivity of the cutting tool (AlTiC) used was 20 W/m K.

In new tool cutting, only the shear plane heat source contributes to the temperature rises at the machined-surface. Typical workpiece temperature contours are shown in Figs. 7 and 8, in an axial cross-sectional view (YZ plane)

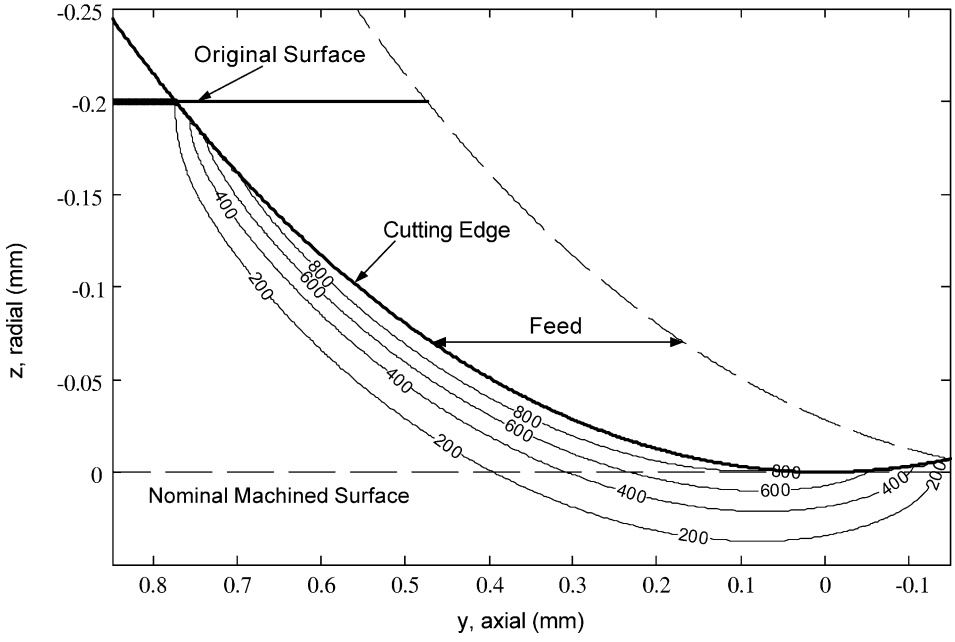

Fig. 7. Temperature contours (in °C) around the cutting edge, new tool cutting.

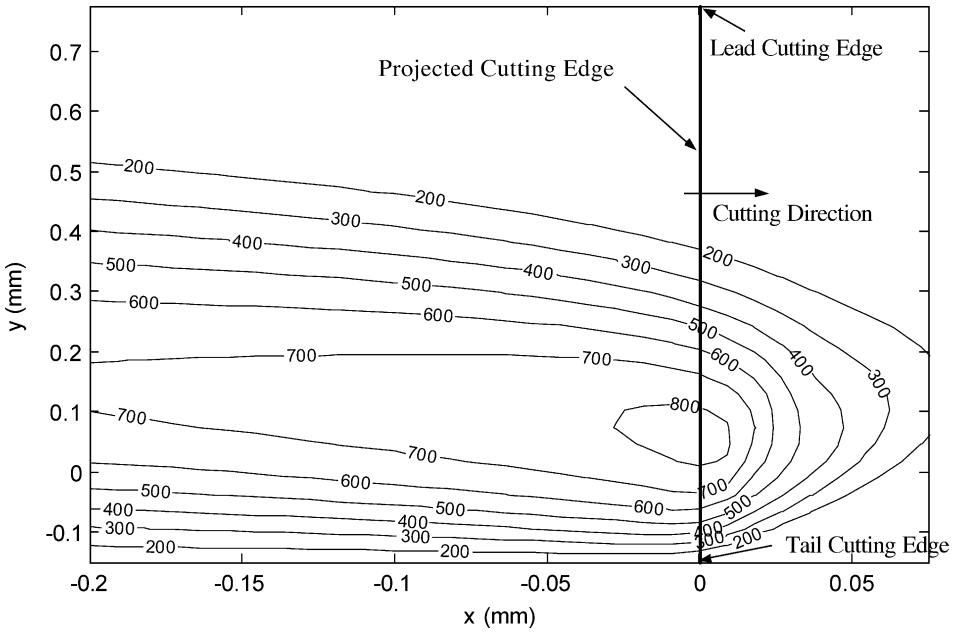

Fig. 8. Temperature contours (in °C) at the nominal machined-surface, new tool cutting.

and the machined-surface view (*XY* plane), respectively; see Fig. 3 for definition. Cutting conditions are 2 m/s cutting speed, 0.3 mm/rev feed, 0.2 mm depth of cut, and 1.6 mm nose radius. Temperature distributions across the cutting edge are not uniform, especially around the lead and tail cutting edges. It is further evident that the tail cutting edge temperatures are far more critical to the machined-surface temperatures in finish hard turning than other portion of the cutting edge.

Figs. 9 and 10 show, in worn tool cutting, temperature contours in an axial cross-sectional view (*YZ* plane) and the machined-surface view (*XY* plane), respectively. Cutting conditions are 0.1 mm wear-land width, 2 m/s cutting speed, 0.3 mm/rev feed, 0.2 mm depth of cut, and 1.6 mm nose radius. Note that 0.3 mm/rev feed rate is not practically used in hard turning (possible fracture), but analyzed here only for comparison purpose (with new tool cutting) to demonstrate the wear-land effects; some values exceeding melting point may be unreasonable. Significant increase of machined-surface temperatures due to wear-land rubbing can be observed by comparing the new tool results.

The developed thermal model has been used to systematically analyze machining temperatures in finish hard turning. For new tool cutting, Fig. 11 shows cutting speed and feed rate effects on the maximum temperature at the nominal machined-surfaces. Machining conditions

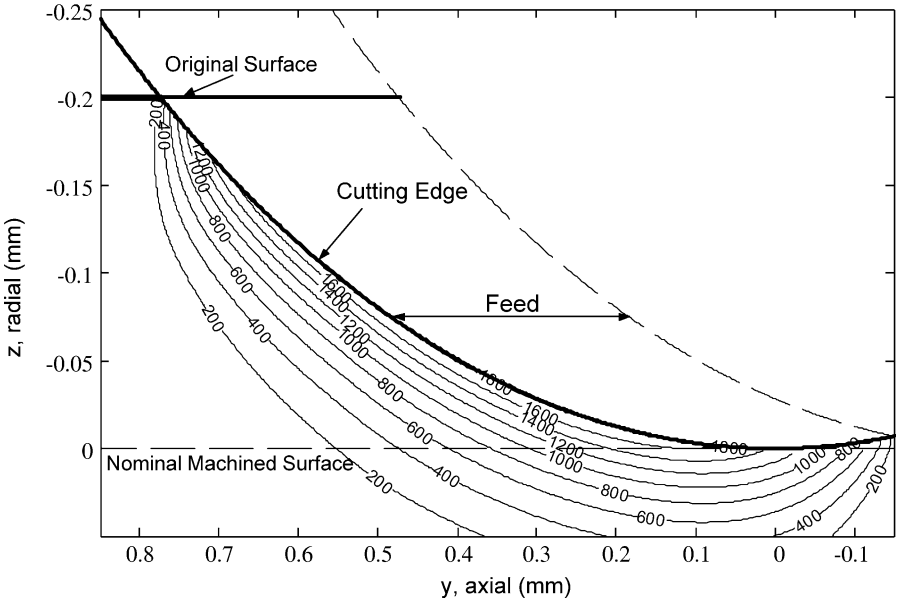

Fig. 9. Temperature contours (in °C) around the cutting edge, 0.1 mm VB.

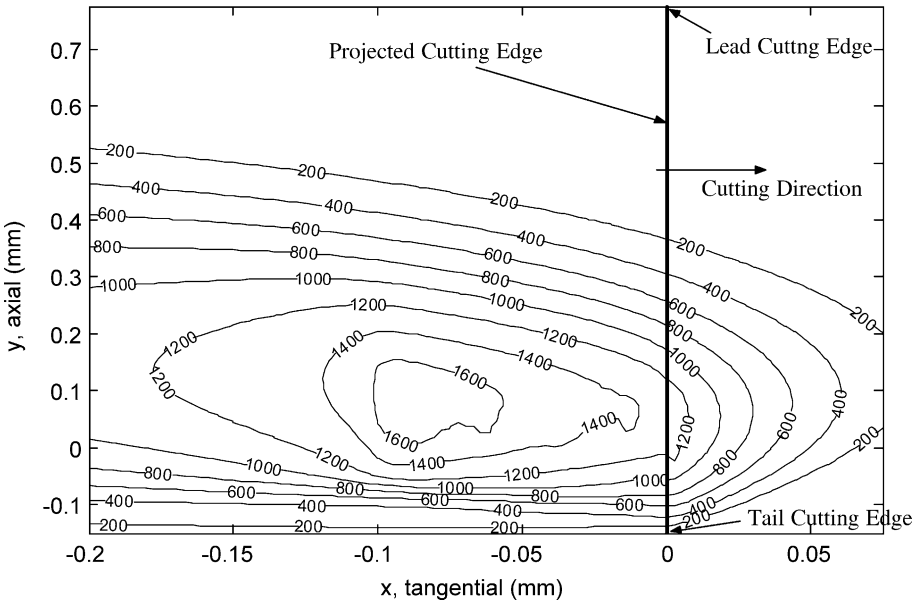

Fig. 10. Temperature contours (in °C) at the nominal machined-surface, 0.1 mm VB.

include 1–4 m/s cutting speed, 0.05–0.3 mm/rev feed rate, 0.1–0.3 mm depth of cut, and 0.8 mm tool nose radius. The maximum machined-surface temperature increases with both cutting speed and feed rate. The maximum machined-surface temperature, on the other hand, moderately decreases with depth of cut as shown in the Fig. 12. Part surface temperatures increase with cutting speed and feed rate because of a greater heat flux. However, heat flux does not increase with the depth of cut. As the depth of cut increases, the shear angle increases as well, and the shear plane heat source effects on the machined-surface are lesser because of a greater distance from the shear plane to the cut surface. Further, increasing depth of cut only makes the leading cutting edge farther away from the nominal machine surface, and, thus, has little effects on the machined-surface temperatures.

For worn tool cutting, cutting conditions tested include 1–6 m/s of cutting speed, 0.1–0.3 mm of wear-land width, 0.05–0.15 mm/rev of feed rate, 0.1–0.3 mm of depth of cut, and 0.8–2.4 mm of tool nose radius. Fig. 13 shows maximum machined-surface temperatures increasing with cutting speed and wear-land size. Wear-land effects on machined-surface temperatures are substantial, increasing 2–3 times from 0 to 0.2 mm VB. It is also noted that temperature-increasing rates seem to decrease at higher cutting speed and larger wear-land. As in new tool cutting, feed rate has a strong effect on the workpiece temperature rise and wear-land presence does not affect the increasing trend. On the other hand, depth of cut effects on machined-surface temperatures are less significant at all wear-land sizes, Fig. 14, different from new tool cutting results. In worn tool cutting, wear-land heat source may be dominant especially in mild cutting conditions, and increasing depth of cut will only increase the wear-land area, but no change in heat intensity, and, thus, does not significantly affect machined-surface temperatures.

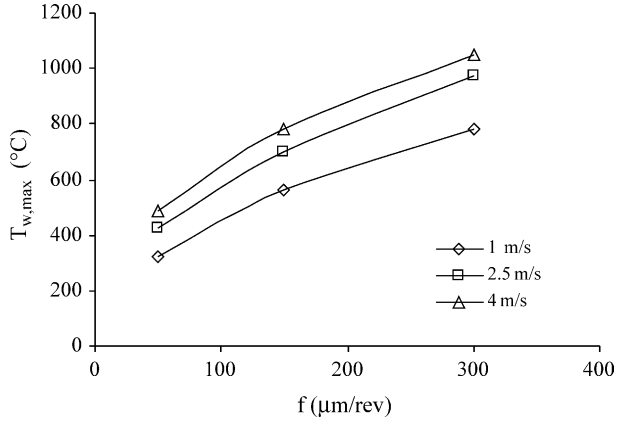

Fig. 11. Cutting speed and feed rate effects on maximum machined-surface temperatures (new tool cutting, $d=0.2$ mm).

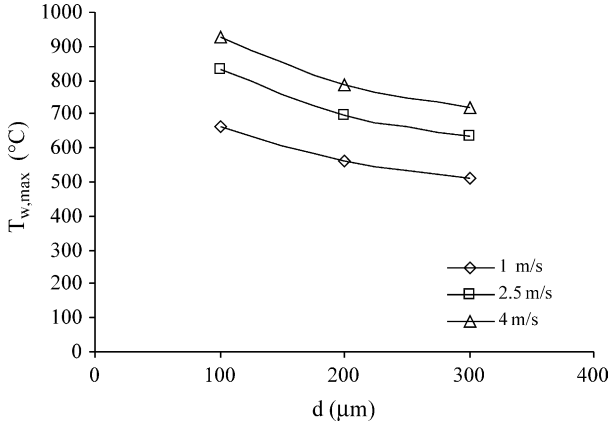

Fig. 12. Depth of cut effects on maximum machined-surface temperatures (new tool cutting, $f=0.15$ mm/rev).

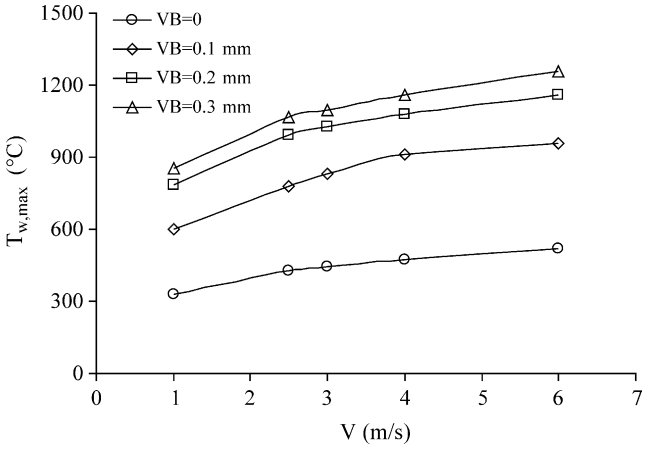

Fig. 13. Cutting speed and flank wear effects on maximum machined-surface temperatures (f=0.05 mm/rev, d=0.2 mm).

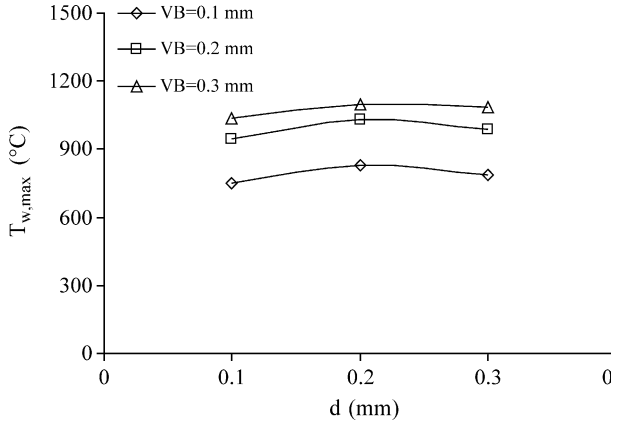

Fig. 14. Depth of cut and flank wear effects on maximum machined-surface temperatures (V=3 m/s, f=0.05 mm/rev).

Heat partition coefficients have also been evaluated. Fig. 15 shows that β_w decreases with increasing cutting speed, but nearly constant to VB, at least in the tested range, 0.1–0.3 mm. In most cases, β_w also slightly decreases with feed rate, but slightly increases with depth of cut. For different feed rates and depths of cut, wear-land size affects β_w insignificantly except at high feed rate and low depth of cut. Given cutting conditions in the current study, β_w ranges from 5 to 15% to the tool. On the other hand, β_r decreases with increasing wear-land size (Fig. 16), less than 10%, and effects of other machining parameters on β_r have the same tendency as in new tool cutting.

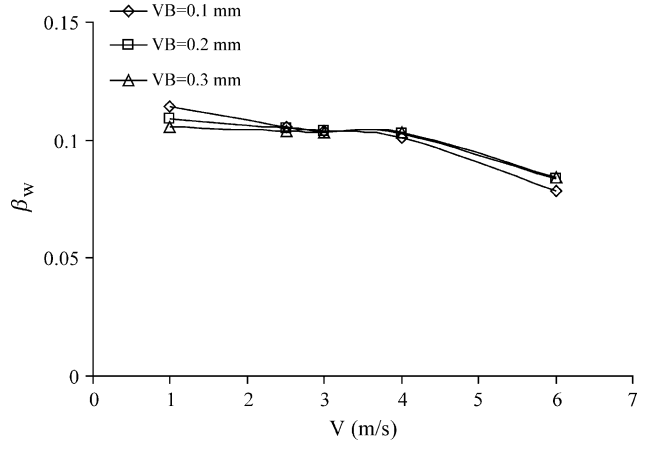

Fig. 15. Cutting speed and flank wear effects on the heat partition coefficient of wear-land heat source (f=0.05 mm/rev, d=0.2 mm).

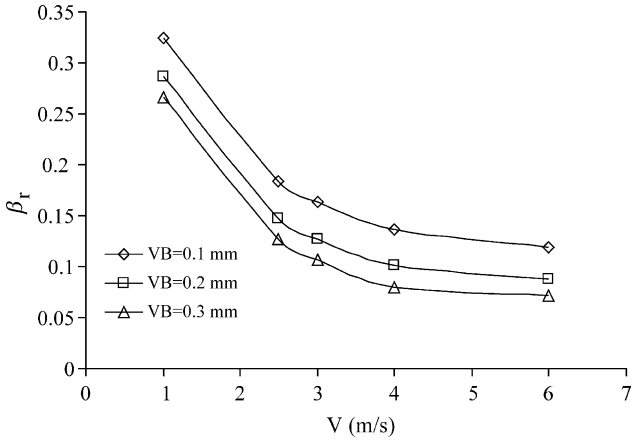

Fig. 16. Cutting speed and flank wear effects on the heat partition coefficient of rake face heat source (f=0.05 mm/rev, d=0.2 mm).

The model has also been used to estimate white layer depth in finish hard turning by computing the penetration depth of the phase transformation temperature (727 °C) at machined-surfaces. Cutting speed and wear-land effects are evaluated. Fig. 17 shows predicted white layer depths vs. cutting speed and wear-land width. It should be noticed that the dash lines in the figure, simply point connections, do not imply exact maximum and corresponding conditions of predicted white layer formations. The data points, however, reveal a general trend that white layer depth increases with cutting speed, however, slightly decreases or levels off once cutting reaches a critical speed. This finding is in qualitative agreement with the results of an earlier study [3]. In moving heat source problems, higher cutting speeds result in higher

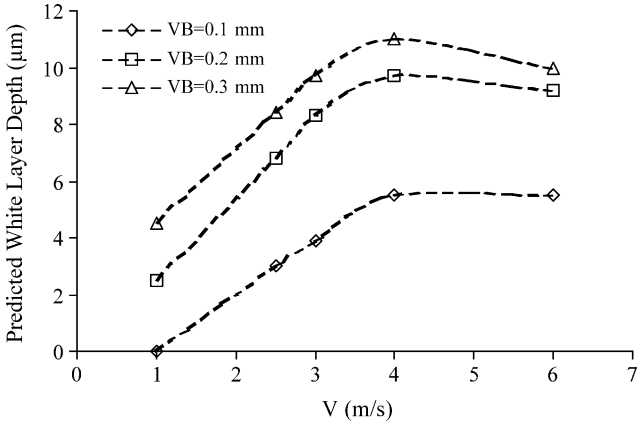

Fig. 17. Predicted white layer (WL) depth as a function of cutting speed at different wear-land sizes (f=0.05 mm/rev, d=0.2 mm).

heat intensity (assuming constant sliding force) as well as greater temperature gradient along the depth. The analysis results imply that at low cutting speed, the heat intensity effect is dominant. However, when cutting speed is higher than a critical value, the temperature gradient effects become more influential to the heat penetration depth.

5. Experimental investigations

For verification of the mechanistic force model, another 18 hard turning experiments have been conducted and compared with the model predictions. The predicted tangential forces (F_t) agree with experimental data fairly well, mostly being less than 10%, Fig. 13. Errors of the radial (F_r) and axial (F_a) components are relatively larger, with maximum about 20–30% [19]. Selected machining conditions were continuously used to generate tool wear with cutting forces recorded. Cutting conditions tested were 3 m/s of cutting speed, 0.2 mm depth of cut, 0.05 mm/rev feed rate, and 0.8–2.4 mm tool nose radius. Cutting forces due to wear-land were obtained by subtracting the corresponding fresh tool cutting forces from measured total cutting forces. The experimental results of tangential wear-land forces show linear correlation with VB and agree with the predictions well, with relative errors less than 15%. Modeled tangential forces, hence, ensure accurate estimate of wear-land heat intensity. Comparing to the tangential component, the errors of radial forces are relatively large, though still less than 30% [20].

5.1. Machined-surface temperatures

The developed thermal model can be used to predict part thermal damage, e.g. white layer formations. With the assumption that the white layer in steel machining is the phase transformation (austenitization) product, white layer depth could be used to estimate the penetration depth of austenitizing temperature at the machined-surface. Similar approach, changes in microstructure of steel tools, has been used to assess cutting tool temperatures [23].

Hard turning test was conducted to investigate tool nose radius effects on the white layer formations and to validate the analytical model. Machining parameters that were kept constant include 2 m/s cutting speed and 0.2 mm depth of cut. Fig. 18 shows, in new tool cutting, white layer depth vs. tool nose radius at different feeds. Experimental data was from two replicates, plotted with average and the range of two results. White layer depth measurements were taken at the nominal machined-surfaces (surface profile valley). In general, white layer depth decreases with increasing tool nose radius. The analytical predictions show good agreement with experimental results. White layer depths also increase with feed rate due to larger chip load, and, thus, greater heat generation rates.

Experiments were continuously conducted for machining temperature comparison in finish hard turning using a worn tool. The developed thermal model was employed to analyze the penetration depth of the austenitizing temperature at each cutting condition. Fig. 19 compares white layer depths between the model predictions and experimental results. White layer depth seems to slightly decrease with tool nose radius at small wear-land, but increase with tool nose radius at large wear-land. The model consistently underestimates white layer depth at large wear-land, but overestimates at small wear-land. This may be attributed to assumptions adopted, e.g. approximation of wear-land geometry. As shown in Fig. 2(b), the boundary of wear-land is defined by angles a and b. The maximum temperature in workpiece and heat penetration depth could be very sensitive to angle b, which is assumed to be 55° in the model. Generally, larger angle b will increase wear-land dimension around the tail cutting edge and result in higher temperatures and consequently a deeper white

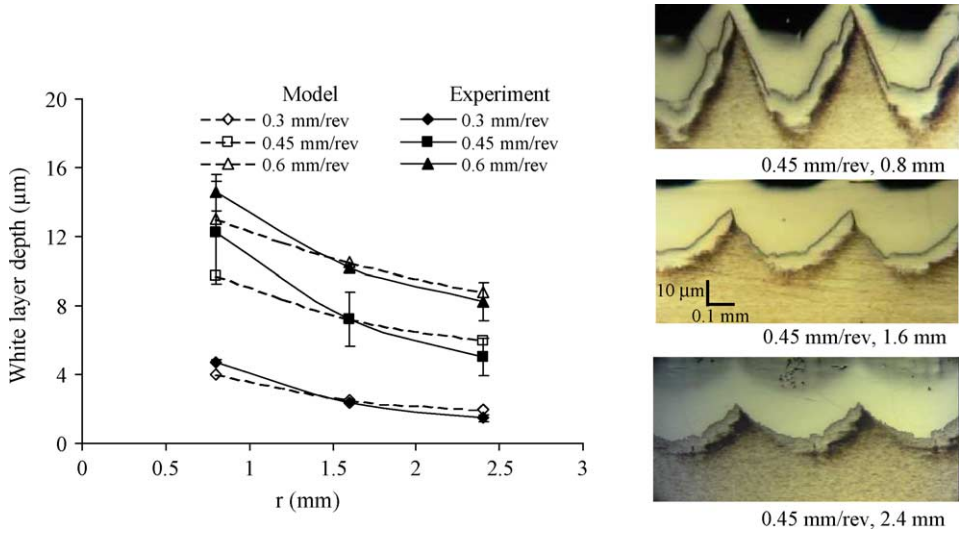

Fig. 18. White layer depth vs. tool nose radius at different feed rates (new tool cutting).

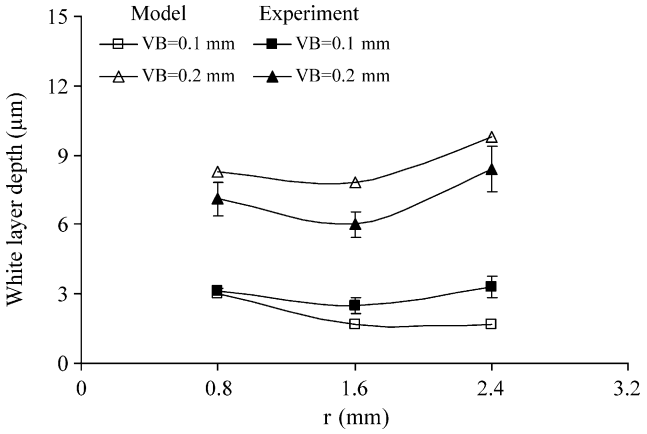

Fig. 19. White layer depth in worn tool cutting, comparison between predictions and experiments.

layer. Nevertheless, the model is able to estimate white layer depth ranges and interpret the trend of tool nose radius effects.

6. Discussion

The thermal model developed in this study primarily applies moving and stationary heat sources approaches, modified from [13,14], and superposition of the results from all individual discretized heat-source segments. This approach, thus, assumes the energy transport phenomenon to be linear, and constant thermal properties are used in the model. However, it is known that thermal properties are dependent on temperatures. Therefore, the thermal properties associated with an equivalent temperature need to be decided and used in the model. Determination of the equivalent temperatures may, therefore, affect the model accuracy. Currently, there seems to have no systematic methods to estimate such equivalent temperatures.

The cutting tool in the analysis was modeled as a semi-infinite body, instead of quarter-infinite as in other studies. A quarter-infinite tool was also tested in the model, however, yielded unreasonably high tool temperatures. Cutting tools used in hard turning usually have a chamfer (e.g. 20°), resulting in a larger tool wedge angle (e.g. 110°) between quarter- and semi-infinite assumptions.

White layer formation was used as an experimental temperature index to compare the model predictions. It has been discussed that white layer formation temperature in hard turning may be deviated from the one in the Fe–C phase diagram [3]. Stresses and strains induced in the machined-surface layer during hard turning may alter the phase transformation temperature from energy consideration. However, such relationship has not been established. Furthermore, the alteration of the phase transformation temperature due to stresses/strains may be smaller compared to possible errors introduced by other simplifications. In addition, the stress/strain magnitudes encountered at the machined-surface are in comparable levels for the machining conditions tested, and, thus, qualitative comparison is considered valid. Machined-surfaces and the cutting zone in finish hard turning subject to high temperatures and temperature gradients, and, currently, there are no reliable measurement techniques for this purpose. Thus, white layer information provides an experimental means as a temperature index to validate the developed model. Uncertainty of white layer measurements has been reported in an earlier study [3]; for a 10 μm white layer sample, the maximum uncertainty is around 1.2 μm, roughly 25–35 °C difference.

This study attempts to establish a framework to analytically investigate cutting temperatures, especially machined-surface temperatures, in finish hard turning considering the shear plane, rake face and wear-land heat sources in three-dimensional machining. The approach requires only limited sets of machining tests to establish mechanistic force model and heat-source geometry which information is subsequently used for temperature calculations and allows systematic investigations of parameter effects. Moreover, the analytical approach demands less computational time and memory to obtain needed temperature information at specific locations or surfaces without the complete information of the entire domain.

In this study, tool wear effects on the shear plane and chip–tool contact are neglected, which is practically debatable. In addition, wear-land geometry has been modeled with simple shape for analysis purpose. It is noted that two angles, a and b, are approximated in a range based on experimental observations. However, the angle b is directly related to the heat-source dimension around the tail cutting edge that has a strong influence to machined-surface temperatures. Thus, the thermal model may be very sensitive to wear-land geometry, especially at the tail cutting edge.

7. Conclusions

An analytical thermal model that includes shear plane, rake face, and wear-land heat sources has been developed for finish hard turning using either a new or worn tool. The objective is to predict cutting temperatures in finish hard turning. Particularly, the machined-surface temperature is addressed for part thermal damage assessment. The methodology was originated from mechanistic cutting force modeling, linear growth of plastic zone on the wear-land, three dimensional cutting geometry, and modified moving and stationary heat-source approaches developed by Komanduri and Hou [13,14]. All heat sources are characterized and subsequently used to compute, simultaneously, cutting temperatures in finish hard turning.

The model has been applied to study process parameter effects on machining temperatures. The results show that, in new tool cutting, maximum machined-surface temperatures

increase with cutting speed and feed rate, but decrease with depth of cut. It has also been shown that flank wear has decisive effects on machined-surface temperatures, maximum temperature increasing 2–3 times from 0 to 0.2 mm wear-land width. The thermal model also predicts that the penetration depth of austenitizing temperature increases with cutting speed, but over a critical speed, seems to become saturated.

The thermal model has also been evaluated by investigating tool nose radius effects on white layer formations for experimental validation. White layer depths predicted by the model qualitatively agree with the experimental results. In new tool cutting, white layer depths decrease with tool nose radius because of a smaller uncut chip thickness. In cutting with a large wear-land, however, it seems that white layer depth increases with tool nose radius because of a shorter distance from the cutting edge to the nominal machined-surface.

The developed model forms a framework for cutting temperature predictions in finish hard turning, especially the machined-surface temperature that is critical to part surface integrity. The model accuracy can be further improved from a few aspects related to adopted assumptions such as ideal wear-land geometry and constant thermal properties, etc. For future work, sensitivity analysis of parameters related to model assumptions will be conducted for error estimate. Cutting temperatures will need to be measured to better validate the model, as well as to guide refinements of the model.

Acknowledgements

HS acknowledged financial support, Graduate Council Fellowship, from the Graduate School at The University of Alabama to carry out this study.

References

[1] T.I. Ei-Wardany, M.A. Elbestawi, Phenomenological analysis of material side flow in hard turning: causes, modeling, and elimination, Machining Science and Technology 2 (1998) 249–251.
[2] G. Poulachon, A.L. Moisan, Hard turning: chip formation mechanism and metallurgical aspects, Journal of Manufacturing Science and Engineering 122 (2000) 406–412.
[3] Y.K. Chou, C.J. Evans, White layers and thermal modeling of hard turned surfaces, International Journal of Machine Tools and Manufacture 39 (1999) 1863–1881.
[4] W. König, A. Berktold, K.F. Koch, Turning vs. grinding—a comparison of surface integrity aspects and attainable accuracies, Annals of CIRP 42 (1) (1993) 39–43.
[5] H. Tönshoff, H.-G. Wobker, D. Brandt, Tribological aspects of hard turning with ceramic tools, Journal of the Society of Tribologists and Lubrication Engineers 51 (2) (1995) 163–168.
[6] D.J. Waldorf, R.E. DeVor, S.G. Kapoor, A slip-line field for ploughing during orthogonal cutting, Transaction of ASME, Journal of Manufacturing Science and Engineering 120 (1998) 693–699.
[7] D.W. Smithey, S.G. Kapoor, R.E. DeVor, A worn tool cutting force model for three-dimensional cutting operations, International Journal of Machine Tools and Manufacture 40 (2000) 1929–1950.
[8] D.W. Smithey, S.G. Kapoor, R.E. DeVor, A new mechanistic model for predicting worn tool cutting forces, Machining Science and Technology 5 (2001) 23–42.
[9] S.V.T. Elanayar, Y.C. Shin, Modeling of tool forces for worn tools: flank wear effects, Transaction of ASME, Journal of Manufacturing Science and Engineering 118 (3) (1996) 359–366.
[10] J.Y. Wang, C.R. Liu, A new concept for decoupling the cutting forces due to tool flank wear and chip formation in hard turning, Machining Science and Technology 2 (1998) 77–90.
[11] J.Y. Wang, C.R. Liu, The effect of tool flank wear on the heat transfer, thermal damage and cutting mechanics in finish hard turning, Annals of the CIRP 48 (1999) 53–58.
[12] Y. Huang, S.Y. Liang, Modeling of CBN tool flank wear progression in finish hard turning, ASME Journal of Manufacturing Science and Engineering 126 (1) (2004) 98–106.
[13] R. Komanduri, Z.B. Hou, Thermal modeling of the metal cutting process—Part I: temperature rise distribution due to shear plane heat source, International Journal of Mechanical Sciences 42 (2000) 1715–1752.
[14] R. Komanduri, Z.B. Hou, Thermal modeling of the metal cutting process—Part II: temperature rise distribution due to frictional heat source at the tool–chip interface, International Journal of Mechanical Sciences 43 (2001) 57–88.
[15] R. Komanduri, Z.B. Hou, Thermal modeling of the metal cutting process—Part III, International Journal of Mechanical Sciences 43 (2001) 89–107.
[16] R.S. Hahn, On the temperature developed at the shear plane in the metal cutting process, Proceedings of First US National Congress of Applied Mechanics, 1951 pp. 661–666.
[17] J.C. Jaeger, Moving sources of heat and the temperature at sliding contacts, Journal and Proceedings Royal Society of New South Wales 76 (1942) 133–228.
[18] S. Asai, A. Kobayashi, Observation of chip producing behavior in ultra-precision diamond machining and study on mirror-like surface generating mechanism, Precision Engineering 12 (3) (1990) 137–143.
[19] Y.K. Chou, H. Song, Thermal modeling for finish hard turning using a new cutting tool, Proceedings of ASME IMECE (International Mechanical Engineering Conference and Exposition), Manufacturing Science and Engineering IMECE-41765, 2003 pp. 16–21.
[20] Y.K. Chou, H. Song, Thermal modeling for finish hard turning using a worn cutting tool, Proceedings of ASME Japan–US Symposium on Flexible Automation, UL_014 (in CD-ROM) Denver, CO, July 19–21 2004.
[21] D.W. Smithey, S.G. Kapoor, R.E. DeVor, A new mechanistic model for predicting worn tool cutting forces, Journal of Machining Science and Technology 5 (2001) 23–42.
[22] Y.S. Touloukian, C.Y. Ho, Thermal Conductivity: Metallic Elements and Alloys, IFI/Plenum, New York, 1970. pp. 1212–1215.
[23] P.K. Wright, Correlation of tempering effects with temperature distribution in steel cutting tools, Transactions of the ASME, Journal of Engineering of Industry 100 (1978) 131–136.